Hybrid layer-by-layer (LbL) films of polyaniline, graphene oxide and zinc oxide to detect ammonia

Rafaela S. Andre [a,b,*], Flávio M. Shimizu [a,c], Celina M. Miyazaki [d], Antonio Riul Jr [e], Danilo Manzani [f], Sidney J.L. Ribeiro [f], Osvaldo N. Oliveira Jr [c], Luiz H.C. Mattoso [a,b], Daniel S. Correa [a,b,**]

[a] National Laboratory for Nanotechnology in Agribusiness (LNNA), Embrapa Instrumentation, 13560-970, São Carlos, SP, Brazil
[b] Center for Exact Sciences and Technology, Department of Chemistry, Federal University of São Carlos (UFSCar), 13565-905, São Carlos, SP, Brazil
[c] São Carlos Institute of Physics (IFSC), University of Sa˜o Paulo (USP), P.O. Box 369, 13566-590 Sa˜o Carlos, SP, Brazil
[d] CCTS, Federal University of São Carlos (UFSCar), Sorocaba, SP, Brazil
[e] Institute of Physics Gleb Wataghin, Unicamp, 13083-859, Campinas, SP, Brazil
[f] Institute of Chemistry, São Paulo State University (UNESP), 14801-970, Araraquara, SP, Brazil

ABSTRACT

Reliable gas sensors operating at room temperature are in demand for monitoring the environment for hazardous pollutants, such as ammonia (NH_3) gas that may become toxic to humans and animals above a threshold concentration. In this paper we report on the combination of three materials, namely polyaniline (PANI), graphene oxide (GO) and zinc oxide (ZnO), to produce hybrid layer-by-layer (LbL) films used for sensing NH_3 with impedance spectroscopy measurements. The deposition of tetralayered PANI/GO/PANI/ZnO LbL films was confirmed with UV–vis. absorption and Raman spectroscopies, while atomic force microscopy (AFM) served to investigate film morphology. Exposure of these LbL films to NH_3 caused film roughness to vary, in an effect that depended on the number of tetralayers. Because of synergy in the materials properties, the films with 3 tetralayers were found to be the most adequate for detecting NH_3 in the range from 25 ppm to 500 ppm with a response time of 30 s. These figures of merit are adequate for monitoring working environments regarding gas exposure, and highlight the usefulness of the control of film architecture provided by the LbL technique.

© 2016 Elsevier B.V. All rights reserved.

1. Introduction

Sensitive, reliable gas sensors have great importance in medical applications, air quality supervision and environmental, health and safety monitoring [1–8]. Ammonia is a colourless gas used in many industries, which may become toxic and affect the health of humans and animals, such as in poultry farms [9,10]. For instance, 100–200 ppm of ammonia induce drowsiness, salivation and loss of appetite in humans [11,12]. According to the regulatory agency in Brazil, the ammonia exposure level at working places should not exceed 20 ppm within 48 h/week [13], while in England the ammonia exposure should not exceed 25 ppm in 8 h [14]. The human olfactory limit of detection for ammonia is 55 ppm, but loss of sensitivity occurs after long and repeated exposure [15–17]. Therefore, designing robust ammonia sensors with low limits of detection is necessary to increase safety and health in such environments [18]. The working principle of gas sensors can be based in changes of electrical and optical properties, with those exploiting electrical signal variations the most used since stable and reproducible sensors can be fabricated [19]. In particular, a myriad of materials can be exploited to achieve such task, including metal oxide semiconductors, conducting polymers, composite materials, carbon nanotubes and their derivatives [4,18,20–24].

In this paper, we report on sensing units made with nanostructured layer-by-layer (LbL) films [25–30] containing the semiconducting polyaniline (PANI), graphene oxide (GO) and zinc oxide (ZnO), all of them already used in sensing applications. The main motivation is to rationally combine different materials in a single device originated from a possible synergy of the materials properties. PANI has unique electrical behavior, easy fabrication process and intrinsic redox reaction [31–37]. ZnO has remarkable
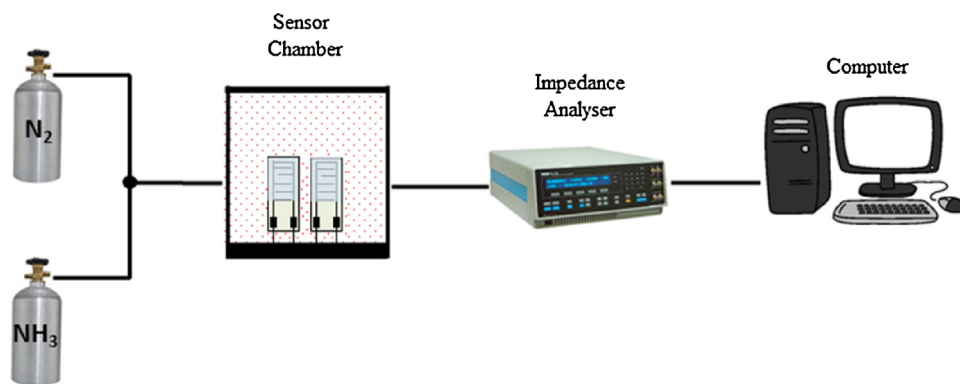
Fig. 1. Schematic diagram of the experimental setup for NH_3 detection.

semiconducting properties [38–41], and GO has a porous structure, high surface area and good gas barrier properties [42–44]. Different LbL film architectures were tested for NH_3 sensing using impedance spectroscopy, which were also characterized using UV–vis absorption spectroscopy, scanning electron microscopy, atomic force microscopy and Raman spectroscopy.

2. Experimental

2.1. Materials

Polyaniline (PANI, Mw = 20.000 g mol^{-1}) was purchased from Sigma-Aldrich. ZnO nanoparticles were synthesized using the coprecipitation method followed by hydrothermal treatment at 150 °C for 1 h as described in Ref [45]. Graphene oxide (GO) was prepared by typical Hummers' method [46] with a previous preoxidation step [47]. The dispersing agent Liosperse 511 was purchased from Miracema-Nuodex (Campinas, Brazil). Gold interdigitated microelectrodes (IDEs) comprising 50 pairs of digits having 10 μm width and 10 μm apart from each other were fabricated by photolithography at the Brazilian Nanotechnology National Laboratory (LNNano).

2.2. Preparation of PANI/GO/PANI/ZnO LbL films

PANI solution (1 mg/mL) was prepared by dispersing the emeraldine base in 1 mL of dimethylacetamide (DMAc) under stirring for 12 h. The solution was then filtrated using a filter paper (80 g/m^2 and pores with 8 μm) purchased from J Prolab. Next, PANI solution was mixed with HCl excess (1:9 v:v) at pH = 3.0. GO was dispersed similarly in HCl solution at 0.1 mg mL^{-1} (pH = 3.0). The dispersion of ZnO nanoparticles (1 mgmL^{-1}) was prepared using distilled water and the dispersing agent (0.5% in relation to total volume) (pH = 8.0). Layer-by-Layer (LbL) films of PANI/GO/PANI/ZnO was deposited onto quartz plates and IDEs by sequential alternated immersions into PANI (cationic solution), GO (anionic solution), PANI and ZnO (anionic solution) until the formation of 2, 3 and 4 tetralayers (PGPZ2T, PGPZ3T and PGPZ4T).

2.3. Multilayer films characterization

The adsorption of LbL multilayers deposited on quartz slides was monitored by UV–vis absorption spectroscopy using a Perkin-Elmer Lambda 25 spectrometer. The morphology of the LbL films was evaluated using a scanning electron microscope (SEM, JEOL 6510) operating at 10 kV. The topography, roughness (root mean square value) and homogeneity of the LbL films were assessed by Atomic Force Microscopy (AFM) using a Dimension V (Veeco) microscope. The Raman spectra of the LbL films were taken at room
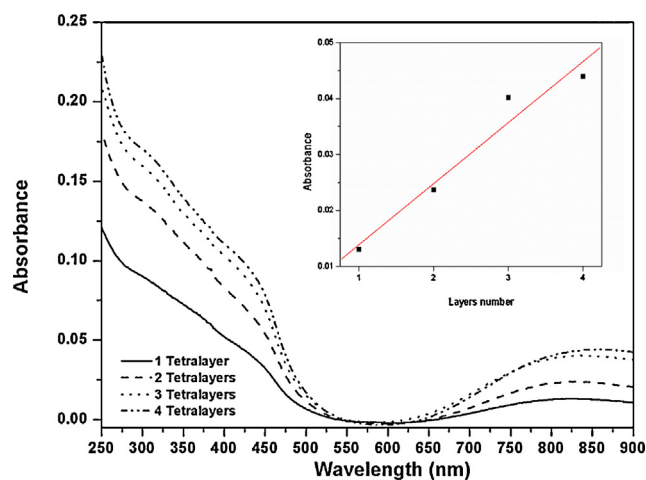

Fig. 2. Absorption spectra of LbL films (PGPZ2T, PGPZ3T and PGPZ4T). Inset displays the absorption peak intensity at 840 nm versus the number of deposited tetralayers.

temperature with a Horiba Jobin-Yvon micro Raman spectrometer model LabRAM-HR equipped with a 632.8 nm laser delivering 30 mW.

2.4. Electrical measurements

Electrical characterization of the sensing units made with the LbL films deposited on IDEs was performed using an impedance analyzer (Solartron, model 1260). Data were collected in the frequency range from 1 Hz up to 1 MHz, using an *ac* applied voltage of 25 mV. The sensors were tested for NH_3 detection, in concentrations ranging from 25 ppm up to 500 ppm, in a closed chamber at room temperature (24 ± 2 °C) in relative humidity of 65 ± 2% with a dynamic gas flow system in the homemade setup schematically displayed in Fig. 1. High purity N_2 was used as carrying gas for NH_3 flux.

3. Results and discussion

Fig. 2 shows the UV–vis spectra of tetralayered LbL films, with absorption bands at 320 and 840 nm, assigned respectively to the π-π^* electronic transition of the benzene ring of amine groups and π-π^* transition of graphene (at approximately 290 nm) [48], and polaronic band of doped PANI in its conductive emeraldine form [36]. The linear increase of the absorpion peak intensity at 840 nm with the number of tetralayers reveals that the same amount of material was deposited at each deposition step.
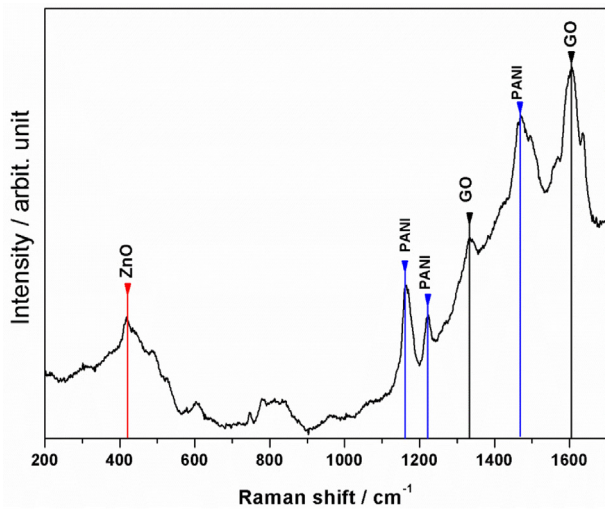
Fig. 3. Raman spectrum of PGPZ4T film.

Table 1
Parameters of the equivalent circuit used to fit the impedance data with ZView®
software (Scribner Associates Inc.).

Film	$R_1(\Omega)$	$R_2(\Omega)$	C_1 (F)	QPE_1n
PGPZ2T	437.6	5524	8.78×10^{-13}	0.0832
PGPZ3T	460.5	2419	9.14×10^{-11}	0.0850
PGPZ4T	387.2	1133	1.23×10^{-12}	0.1410

The presence of GO and PANI was inferred in the Raman spectrum in Fig. 3. The bands assigned to GO appear at $1333\,cm^{-1}$ and $1604\,cm^{-1}$, due to the breathing mode of k-point photons of A_{1g} symmetry and E_{2g} phonon of sp^2 carbon atoms, respectively [48]. The PANI Raman bands appear at $1470\,cm^{-1}$ assigned to C=N stretching vibrations, while the band at $1222\,cm^{-1}$ corresponds to C—N stretching in polaronic units and at $1160\,cm^{-1}$ assigned to C—H in plane bending vibrations of benzenoid ring [24]. The ZnO nanoparticles show only one weak Raman band at $416\,cm^{-1}$ assigned to phonons of ZnO compounds with hexagonal structures [43,49].

The frequency dependence of the impedance real part (Z' (ohms)) is shown in Fig. 4a for the three PGPZ LbL films with 2–4 tetralayers. The impedance spectra were fitted with an equivalent electrical circuit shown in Fig. 4c, comprising the resistor R_1 representing the ohmic resistance from the interdigitated electrode (IDE), R_2 the film resistance and C_1 the capacitance of charge transfer across the multilayer film, in addition to a phase constant element that was included to improve fitting. The data in the form of Nyquist plots in Fig. 4b for the three films in an inert atmosphere with 65% of humidity were fitted with the parameters displayed in Table 1. Both resistances decreased with the number of deposited tetralayers, possibly due to the increase in PANI amount since GO is insulating. A schematic representation of the PANI/GO/PANI/ZnO film deposited onto the IDE is displayed in Fig. 4(d).

The AFM images in Fig. 5 highlight two main features: i) before NH_3 exposure, the film roughness increased with the number of tetralayers, from 35 nm (PGPZ2T) up to 52 nm (PGPZ4T); ii) after exposure to the NH_3, film morphology was clearly affected. Specifically, the thinnest PGPZ2T film was probably deeply penetrated by ammonia, causing both dedoping of PANI and increase in surface roughness. On the other hand, the thicker films with larger amount of PANI had their roughness decreased after ammonia exposure, particularly for the thickest PGPZ4T, whose roughness decreased by ∼40%. Significantly, Fig. 6 indicates that the PGPZ3T was only weakly affected by ammonia. It seems therefore that opposite
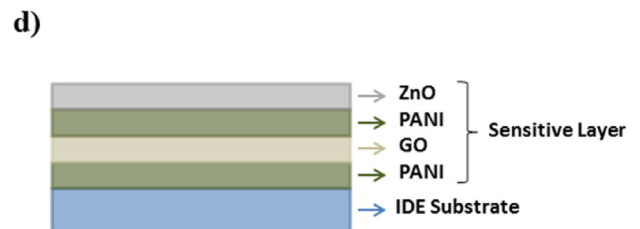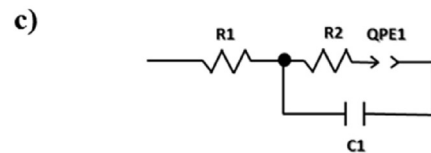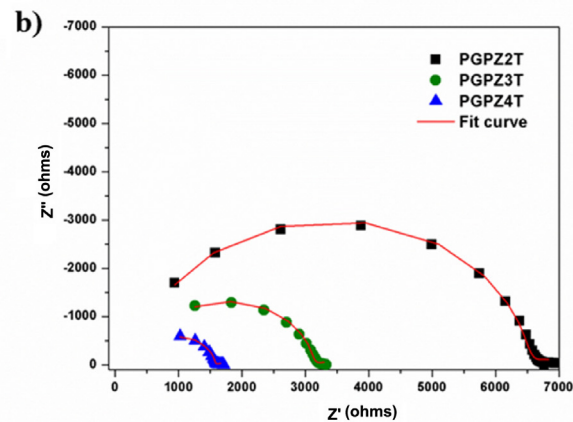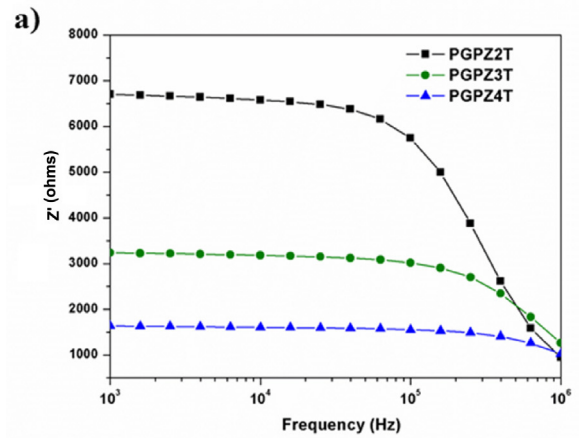

Fig. 4. a) real part of impedance (Z') and b) Nyquist diagram for PGPZ2T, PGPZ3T and PGPZ4T films, c) equivalent circuit model and d) schematic representation of the PANI/GO/PANI/ZnO film deposited onto the IDE.

effects to alter film thickness occur for PGPZ3T, which is associated with synergy in the different materials properties. As it will be shown later, such synergy is responsible for the higher sensitivity of PGPZ3T.

The sensor units made of 2, 3 and 4 tetralayers of PANI/GO/PANI/ZnO were tested for detecting ammonia (NH_3) in a relative humidity (RH) set as 65%. The choice of this humidity value was made because previous investigations reported in the literature [50,51] indicated that the ideal relative humidity in broiler poultry houses should range between 50 and 70%; lower values
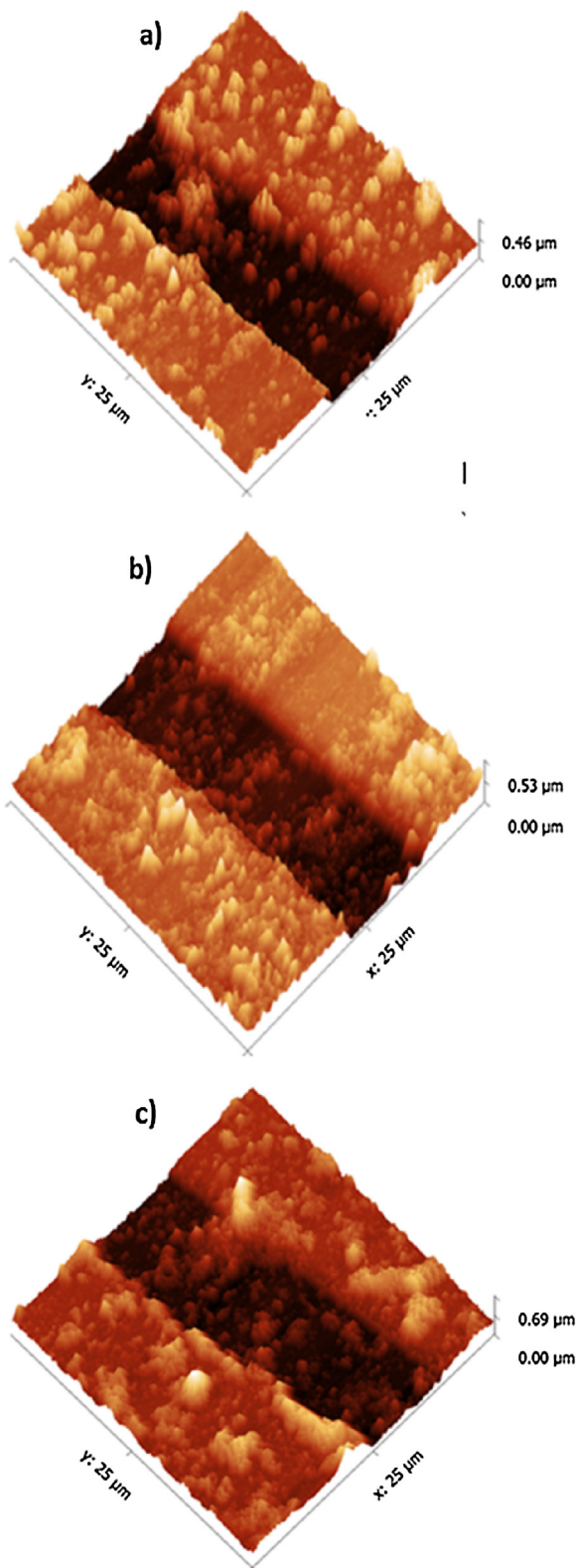
Fig. 5. AFM 3D images of a) PGPZ2T, b) PGPZ3T and c) PGPZ4T films.

Fig. 6. Film roughness (R_{rms}) calculated using Gwyddion® software for LbL films (PGPZ2T, PGPZ3T and PGPZ4T) before and after exposure to ammonia gas.

less affected by ammonia, according to the AFM results, combined with the moderate resistive response of PANI/GO/PANI/ZnO sensitive layer (cf. Table 1). One would expect that the film with larger morphological changes upon NH_3 exposure would yield the highest sensing performance. However, the sensing mechanism appears to depend on a combination of the charge transfer property of the three materials. ZnO [18,52–55] is a *n*-type semiconductor and PANI is a semiconducting polymer, both allowing charge mobility that hinder formation of a stable double layer at the interface. In contrast, GO is an insulator that provides the stability needed for the charge transfer phenomenon in gas sensor application.

$$\text{Response} = Z'_{NH_3}/Z'_{air} \tag{1}$$

It should be noted that for low NH_3 concentrations the sensing units exhibited similar responses, with low error associated to the measurements. That is an important issue to develop sensors able to detect NH_3 below 50 ppm [15–17]. In addition, the larger errors at higher concentrations of NH_3 may be associated with the lower stability of the measuring system, since gas injection can cause small turbulences in the airflow system, as observed in the calibration curve of Fig. 7b. The response time for each NH_3 concentration range was calculated using Eq. (2) to fit the calibration curve in Fig. 7b, leading to values ranging from 10 to 30 s. It is worth mentioning that the fitting required the use of two exponential functions in Eq. (2), which points to more than one process ruling in the sensing mechanism.

$$R(t) = y_0 + A_1 \left(1 - e^{-t/t1}\right) + A_2 \left(1 - e^{-t/t2}\right) \tag{2}$$

R(t) is the resistance as a function of time (t), y_0, A_1 and A_2 are constants, and t_1 and t_2 are the response times.

Response times ranging values from 10 to 30 s are suitable for a device operating at room temperature, since NH_3 gas diffusion and sensing usually occur in a time scale shorter than 30 s [20,56].

Statistical analysis of the impedance data was carried out using PEx-Sensors software[57–59], implementing multidimensional projection techniques. Here we used IDMAP (Interactive Document Map) with Euclidian distances between the data points and employing real impedance data dimensionally reduced by the Fastmap technique in the frequency range $10^3–10^6$ Hz. The IDMAP plot in Fig. 8 confirms that all of the three sensors produced were effective to detect ammonia levels from 50 up to 500 ppm, with a combined silhouette coefficient of 0.64 (separate values of 0.60 for PGPZ2T, 0.59 for PGPZ3T and 0.54 for PGPZT4T), calculated according to Paulovich et. al [58]. With this quantitative measure of

can result in a dusty house, while higher values could result in wet litter and higher ammonia concentrations.

The relative response in terms of the impedance ratio (Eq. (1)) increased with NH_3 concentration up to 500 ppm, as shown in Fig. 7a. PGPZ3T exhibited the most adequate response for all concentrations tested, which may be related to its morphology being
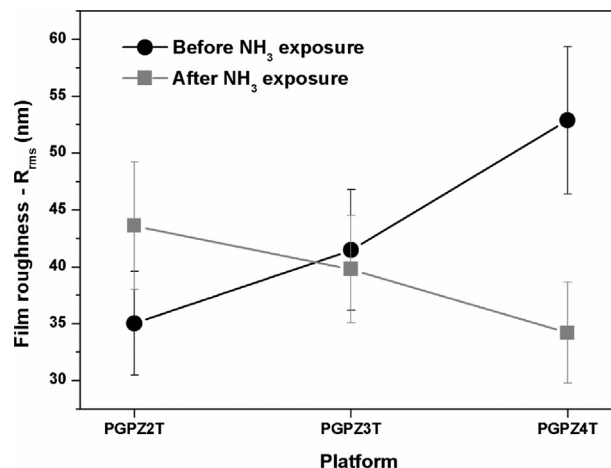
a)

b)

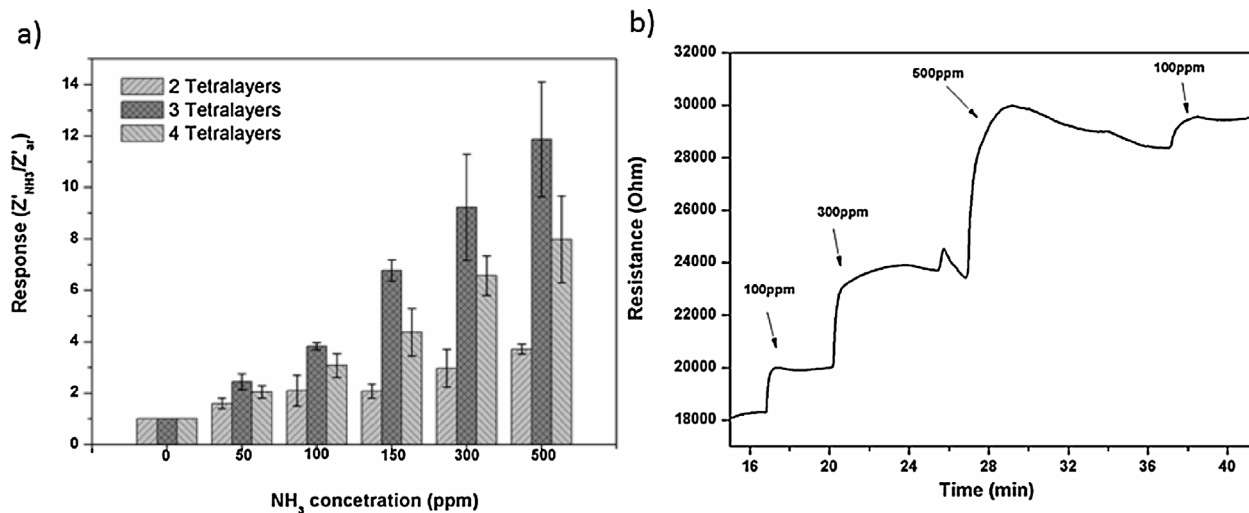**Fig. 7.** a) Sensor responses at different concentrations of NH$_3$ and b) change in electrical resistance as a function of time upon NH$_3$ exposure of a sensing device with PGPZ3T.
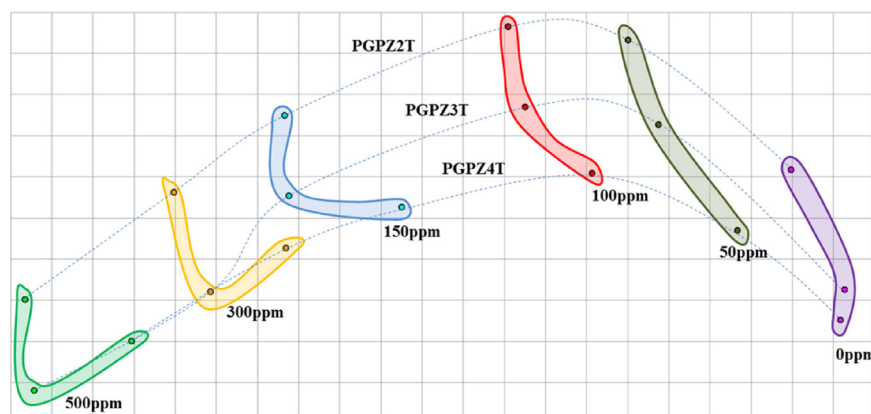

Fig. 8. IDMAP plot obtained with the real component of the impedance data as a function of frequency for PGPZ2T, PGPZ3T and PGPZ4T films. The axes have no labels because what matters in this type of plot is the relative distance between data points. The dashed lines linking data points for each of the sensing units were only included to guide the eyes, and demonstrate the distinction between different NH$_3$ concentrations.

Table 2
Comparison of sensor performance for detecting NH$_3$, where lists are given of the material used in the sensing device, detection limit (DL), response time (RTime), percentage of response. The values quoted for PANI/GO/PANI/ZnO correspond to PGPZ3T.

Material	Detection Limit (DL)	Response Time (RTime)	Response (%)	Ref
PANI/GO/PANI/ZnO	23 ppm	30 s (100 ppm)	38.31	This work
PANI/GO	1 ppm	50 s (100 ppm)	11.33	[20]
TiO$_2$/PPy/GN	1 ppm	36 s (50 ppm)	36	[63]
PANI/αFe$_2$O$_3$	5 ppm	27 s (100 ppm)	39	[64]
PPy/SnO$_2$	257 ppb	259 s (5 ppm)	30	[65]
PANI/SnO$_2$	1.8 ppm	34 s (100 ppm)	29	[66]

the discriminating power of a sensing device, PGPZ3T and PGPZ2T appear as the most adequate molecular architectures.

Regarding to ammonia sensors recently reported, Table 2 shows that the sensors made with tetralayered LbL films are competitive both in terms of response time and magnitude of the detection. Significantly, the figures of merit of the sensors presented here are an adequate choice for target applications, such as monitoring work places for excessive NH$_3$ exposure. Furthermore, the sensor response remained stable up to 15 days, while a decay of 56% on response signal was observed 30 days later.

Although one should expect that a platform based solely on PANI and ZnO (PANI/ZnO) combination could be adequate for sensing application, as PANI presents high sensitivity at room temperature [60] while ceramic materials may provide suitable response

time for sensing application [24,61], this was not found to be the case. Subsidiary experiments (results not shown) employing solely PANI/ZnO platform (without GO) showed to be sensitive to NH$_3$ but with a highly unstable electrical response, which is not adequate for gas sensing application. Therefore, the incorporation of GO to the nanostructured platform definitely improved the sensor response, which is consistent with findings of the literature [62]. Furthermore, PANI/GO/PANI/ZnO platform not only showed improved sensitivity to NH$_3$ but also enhanced stability, reproducibility and fast response. This behavior can by ascribed to the synergy in the electrical properties of the three composing materials, as described before. Therefore, the results demonstrate the importance of adding GO to the PANI/ZnO platform, exploiting molecular combinations of three distinct materials in the same

platform, which allowed the sensor operation at room temperature with fast response and high sensitivity.

4. Conclusions

Tetralayered LbL films could be produced with PANI, GO and ZnO, with the presence of all components being confirmed with UV–vis. absorption and Raman spectroscopies. The number of tetralayers for the PANI/GO/PANI/ZnO architecture affected the electrical properties and morphology, according to impedance spectroscopy data and AFM images, respectively. The overall electrical resistance of the film decreased with the number of tetralayers owing to an increased amount of the conducting PANI. In contrast, film roughness increased with the number of tetralayers, as expected for nanostructured films. The roughness dependence, however, was not monotonic when exposure to NH_3 was considered, since roughness decreased for PGPZ2T, increased for PGPZ4T, and remained practically constant for PGPZ3T. This indicates synergy in combining the materials properties, which was indeed confirmed by the higher performance of PGPZ3T for detecting NH_3 in impedance spectroscopy measurements. The metrics of interest of the sensors made with the LbL films for use in monitoring working environments, namely limit of detection, response time and amplitude of response, were all adequate. Therefore, these PANI/GO/PANI/ZnO films can be considered as an alternative platform for room temperature NH_3 sensors in which synergy is achieved upon combining distinct materials.

Acknowledgements

References

[1] P.-G. Su, L.-Y. Yang, NH3 gas sensor based on Pd/SnO2/RGO ternary composite operated at room-temperature, Sens. Actuators B Chem. 223 (2016) 202–208, http://dx.doi.org/10.1016/j.snb.2015.09.091.
[2] M. Hasan, M.O. Ansari, M.H. Cho, M. Lee, Electrical conductivity, optical property and ammonia sensing studies on HCl doped Au@polyaniline nanocomposites, Electron. Mater. Lett. 11 (2015) 1–6, http://dx.doi.org/10.1007/s13391-014-4200-9.
[3] S. Cui, S. Mao, Z. Wen, J. Chang, Y. Zhang, J. Chen, Controllable synthesis of silver nanoparticle-decorated reduced graphene oxide hybrids for ammonia detection, Analyst 138 (2013) 2877, http://dx.doi.org/10.1039/c3an36922f.
[4] D.K. Bandgar, S.T. Navale, A.T. Mane, S.K. Gupta, D.K. Aswal, V.B. Patil, Ammonia sensing properties of polyaniline/α-Fe2O3 hybrid nanocomposites, Synth. Metals 204 (2015) 1–9, http://dx.doi.org/10.1016/j.synthmet.2015.02.032.
[5] S. Wagner, E. Angenendt, O. Beletskaya, J. Zeddies, Costs and benefits of ammonia and particulate matter abatement in German agriculture including interactions with greenhouse gas emissions, Agric. Syst. 141 (2015) 58–68, http://dx.doi.org/10.1016/j.agsy.2015.09.003.
[6] A.M. McQuilling, P.J. Adams, Semi-empirical process-based models for ammonia emissions from beef, swine, and poultry operations in the United States, Atmos. Environ. 120 (2015) 127–136, http://dx.doi.org/10.1016/j.atmosenv.2015.08.084.
[7] S. Bittman, K. Jones, R. Vingarzan, D.E. Hunt, S.C. Sheppard, J. Tait, et al., Weekly agricultural emissions and ambient concentrations of ammonia: validation of an emission inventory, Atmos. Environ. 113 (2015) 108–117, http://dx.doi.org/10.1016/j.atmosenv.2015.04.038.
[8] D.S. Correa, E.S. Medeiros, J.E. Oliveira, L.G. Paterno, L.H.C. Mattoso, Nanostructured conjugated polymers in chemical sensors: synthesis, properties and applications, J. Nanosci. Nanotechnol. 14 (2014) 6509–6527, http://dx.doi.org/10.1166/jnn.2014.9362.
[9] Y. Zhao, T.A. Shepherd, H. Li, H. Xin, Environmental assessment of three egg production systems −part I: monitoring system and indoor air quality, Poult. Sci. 94 (2015) 518–533.
[10] S. Ta, Y. Zhao, H. Li, S. Jp, H. Xin, Environmental assessment of three egg production systems − part II. Ammonia, greenhouse gas, and particulate
[11] S.B. Kondawar, P.T. Patil, S.P. Agrawal, Chemical vapour sensing properties of electrospun nanofibers of polyaniline/ZnO nanocomposites, Adv. Mater. Lett. 5 (2014) 389–395, http://dx.doi.org/10.5185/amlett.2014.amwc.1037.
[12] A.H. Navarchian, Z. Hasanzadeh, M. Joulazadeh, Effect of polymerization conditions on reaction yield, conductivity, and ammonia sensing of polyaniline, Adv. Polym. Technol. 32 (2013) 5–9, http://dx.doi.org/10.1002/adv.21356.
[13] Guia Trabalista, NR 15 – Atividades e operações insalubres, Anexo XI – Copyright© 2003–2016 Portal Tributário Editora.
[14] M. Bendahan, P. Lauque, C. Lambert-Mauriat, H. Carchano, J.L. Seguin, Sputtered thin films of CuBr for ammonia microsensors: morphology, composition and ageing, Sens. Actuators B Chem. 84 (2002) 6–11, http://dx.doi.org/10.1016/S0925-4005(02)00004-7.
[15] D. Ponnusamy, S. Madanagurusamy, Porous anatase TiO2 thin films for NH3 vapour sensing, J. Electron. Mater. 44 (2015) 4726–4733, http://dx.doi.org/10.1007/s11664-015-4099-4.
[16] Y. Jia, C. Yan, H. Yu, L. Chen, F. Dong, One-step fabrication of ammonia sensor by electrospinning PS- b −PMA nanofibers on quartz crystal microbalance, Sens. Actuators B Chem. 203 (2014) 459–464, http://dx.doi.org/10.1016/j.snb.2014.06.018.
[17] S. Abdulla, T.L. Mathew, B. Pullithadathil, Highly sensitive, room temperature gas sensor based on polyaniline-multiwalled carbon nanotubes (PANI/MWCNTs) nanocomposite for trace-level ammonia detection, Sens. Actuators B Chem. 221 (2015) 1523–1534, http://dx.doi.org/10.1016/j.snb.2015.08.002.
[18] B. Timmer, W. Olthuis, A. Van Den Berg, Ammonia sensors and their applications—a review, Sens. Actuators B Chem. 107 (2005) 666–677, http://dx.doi.org/10.1016/j.snb.2004.11.054.
[19] X. Liu, S. Cheng, H. Liu, S. Hu, D. Zhang, H. Ning, A survey on gas sensing technology, Sensors 12 (2012) 9635–9665, http://dx.doi.org/10.3390/s120709635.
[20] Z. Wu, X. Chen, S. Zhu, Z. Zhou, Y. Yao, W. Quan, et al., Enhanced sensitivity of ammonia sensor using graphene/polyaniline nanocomposite, Sens. Actuators B Chem. 178 (2013) 485–493, http://dx.doi.org/10.1016/j.snb.2013.01.014.
[21] Y. Li, B. Pathak, J. Nisar, Z. Qian, R. Ahuja, Metal-decorated graphene oxide for ammonia adsorption, EPL Europhys. Lett. 103 (2013) 28007, http://dx.doi.org/10.1209/0295-5075/103/28007.
[22] V. Talwar, O. Singh, R.C. Singh, ZnO assisted polyaniline nanofibers and its application as ammonia gas sensor, Sens. Actuators B Chem. 191 (2014) 276–282, http://dx.doi.org/10.1016/j.snb.2013.09.106.
[23] S.G. Pawar, M.A. Chougule, S.L. Patil, B.T. Raut, P.R. Godse, S. Sen, et al., Room temperature ammonia gas sensor based on polyaniline-TiO2 nanocomposite, IEEE Sens. J. 11 (2011) 3417–3423, http://dx.doi.org/10.1109/JSEN.2011.2160392.
[24] U.V. Patil, N.S. Ramgir, N. Karmakar, A. Bhogale, A.K. Debnath, D.K. Aswal, et al., Room temperature ammonia sensor based on copper nanoparticle intercalated polyaniline nanocomposite thin films, Appl. Surf. Sci. 339 (2015) 69–74, http://dx.doi.org/10.1016/j.apsusc.2015.02.164.
[25] J.E. Oliveira, V.P. Scagion, V. Grassi, D.S. Correa, L.H.C. Mattoso, Modification of electrospun nylon nanofibers using layer-by-layer films for application in flow injection electronic tongue: detection of paraoxon pesticide in corn crop, Sens. Actuators B Chem. 171–172 (2012) 249–255, http://dx.doi.org/10.1016/j.snb.2012.03.056.
[26] A. Manzoli, F.M. Shimizu, L.A. Mercante, E.C. Paris, O.N. Oliveira, D.S. Correa, et al., Layer-by-layer fabrication of AgCl–PANI hybrid nanocomposite films for electronic tongues, Phys. Chem. Chem. Phys. 16 (2014) 24275–24281, http://dx.doi.org/10.1039/C4CP04150J.
[27] F.N. Crespilho, V. Zucolotto, O.N. Oliveira, F.C. Nart, Electrochemistry of layer-by-layer films: a review, Int. J. Electrochem. Sci. 1 (2006) 194–214.
[28] Y. Lvov, H. Haas, G. Decher, H. Moehwald, A. Kalachev, Assembly of polyelectrolyte molecular films onto plasma-treated glass, J. Phys. Chem. 97 (1993) 12835–12841, http://dx.doi.org/10.1021/j100151a033.
[29] G. Decher, J.-D. Hong, Buildup of ultrathin multilayer films by a self-assembly process 1 consecutive adsorption of anionic and cationic bipolar amphiphiles on charged surfaces, Makromol. Chem. Macromol. Symp. 46 (1991) 321–327, http://dx.doi.org/10.1002/masy.19910460145.
[30] G. Decher, Fuzzy nanoassemblies: toward layered polymeric multicomposites, Science 277 (80) (1997) 1232–1237, http://dx.doi.org/10.1126/science.277.5330.1232.
[31] J. Chen, J. Yang, X. Yan, Q. Xue, NH3 and HCl sensing characteristics of polyaniline nanofibers deposited on commercial ceramic substrates using interfacial polymerization, Synth. Metals 160 (2010) 2452–2458, http://dx.doi.org/10.1016/j.synthmet.2010.09.026.
[32] M.P. Prabhakaran, L. Ghasemi-Mobarakeh, G. Jin, S. Ramakrishna, Electrospun conducting polymer nanofibers and electrical stimulation of nerve stem cells, J. Biosci. Bioeng. 112 (2011) 501–507, http://dx.doi.org/10.1016/j.jbiosc.2011.07.010.
[33] Y. Zhang, G.C. Rutledge, Electrical conductivity of electrospun polyaniline and polyaniline-blend fibers and mats, Macromolecules 45 (2012) 4238–4246, http://dx.doi.org/10.1021/ma3005982.
[34] S. Valiavalappil, S. Harinipriya, Electrically conducting nylon 6, 6–polyaniline short composite fibres synthesised by the solvent coagulation method, Synth. Metals 162 (2012) 2027–2032, http://dx.doi.org/10.1016/j.synthmet.2012.10.008.
[extra] matter emissions PubMed commons, Poult. Sci. 94 (2015) 534–543, http://dx.doi.org/10.3382/ps/peu075.Full.

[35] C. Van Tuan, M.A. Tuan, N. Van Hieu, T. Trung, Electrochemical synthesis of polyaniline nanowires on Pt interdigitated microelectrode for room temperature NH3 gas sensor application, Curr. Appl. Phys. 12 (2012) 1011–1016, http://dx.doi.org/10.1016/j.cap.2011.12.006.

[36] A. de Barros, M. Ferreira, C.J.L. Constantino, M. Ferreira, Nanocomposites based on LbL films of polyaniline and sodium montmorillonite clay, Synth. Metals 197 (2014) 119–125, http://dx.doi.org/10.1016/j.synthmet.2014.09.001.

[37] C. Steffens, A. Manzoli, J.E. Oliveira, F.L. Leite, D.S. Correa, P.S.P. Herrmann, Bio-inspired sensor for insect pheromone analysis based on polyaniline functionalized AFM cantilever sensor, Sens. Actuators B Chem. 191 (2014) 643–649, http://dx.doi.org/10.1016/j.snb.2013.10.053.

[38] C.-F. Li, C.-Y. Hsu, Y.-Y. Li, NH3 sensing properties of ZnO thin films prepared via sol-gel method, J. Alloys Compd. 606 (2014) 27–31, http://dx.doi.org/10.1016/j.jallcom.2014.03.120.

[39] M. Khairy, Polyaniline–Zn0.2Mn0.8 Fe2O4 ferrite core–shell composite: preparation, characterization and properties, J. Alloys Compd. 608 (2014) 283–291, http://dx.doi.org/10.1016/j.jallcom.2014.04.130.

[40] M. Sharma, P. Jeevanandam, Synthesis characterization and studies on optical properties of indium doped ZnO, Nanoparticles 53 (2014) 561–565.

[41] S.R. Anton, H.A. Sodano, A review of power harvesting using piezoelectric materials (2003–2006), Smart Mater. Struct. 16 (2007) R1–R21, http://dx.doi.org/10.1088/0964-1726/16/3/R01.

[42] S.S. Varghese, S. Lonkar, K.K. Singh, S. Swaminathan, A. Abdala, Recent advances in graphene based gas sensors, Sens. Actuators B Chem. 218 (2015) 160–183, http://dx.doi.org/10.1016/j.snb.2015.04.062.

[43] S. Gayathri, P. Jayabal, M. Kottaisamy, V. Ramakrishnan, Synthesis of ZnO decorated graphene nanocomposite for enhanced photocatalytic properties, J. Appl. Phys. 115 (2014) 179504, http://dx.doi.org/10.1063/1.4874877.

[44] X. He, L.–l. Wu, J. –j. Wang, T. Zhang, H. Sun, N. Shuai, Layer-by-layer assembly deposition of graphene oxide on poly(lactic acid) films to improve the barrier properties, High Perform. Polym. 27 (2015) 318–325, http://dx.doi.org/10.1177/0954008314545978.

[45] R.S. Andre, A. Pavinatto, L. a. Mercante, E.C. Paris, L.H.C. Mattoso, D.S. Correa, Improving the electrochemical properties of polyamide 6/polyaniline electrospun nanofibers by surface modification with ZnO nanoparticles, RSC Adv. 5 (2015) 73875–73881, http://dx.doi.org/10.1039/C5RA15588F.

[46] J. William, S. Hummers, R.E. Offeman, Preparation of graphitic oxide, J. Am. Chem. Soc. 80 (1958) 1339, http://dx.doi.org/10.1021/ja01539a017.

[47] N.I. Kovtyukhova, P.J. Ollivier, B.R. Martin, T.E. Mallouk, S.A. Chizhik, E.V. Buzaneva, et al., Layer-by-layer assembly of ultrathin composite films from micron-sized graphite oxide sheets and polycations, Chem. Mater. 11 (1999) 771–778, http://dx.doi.org/10.1021/cm981085u.

[48] X. Huang, N. Hu, R. Gao, Y. Yu, Y. Wang, Z. Yang, et al., Reduced graphene oxide-polyaniline hybrid: preparation, characterization and its applications for ammonia gas sensing, J. Mater. Chem. 22 (2012) 22488, http://dx.doi.org/10.1039/c2jm34340a.

[49] A.G. Milekhin, N.A. Yeryukov, L.L. Sveshnikova, T.A. Duda, E.I. Zenkevich, S.S. Kosolobov, et al., Surface enhanced Raman scattering of light by ZnO nanostructures, J. Exp. Theor. Phys. 113 (2011) 983–991, http://dx.doi.org/10.1134/S1063776111140184.

[50] Y. Zhao, H. Xin, T. Shepherd, Thermal environment, ammonia concentrations, and ammonia emissions of aviary houses with white laying hens, Trans. ASABE 56 (2013) 1145–1156, http://dx.doi.org/10.13031/trans.56.10097.

[51] J.A.D. Barbosa Filho, M.L.V. Queiroz, D. de, F. Brasil, F.M.C. Vieira, I.J.O. Silva, Transport of broilers: load microclimate during Brazilian summer, Eng. Agrícola. 34 (2014) 405–412, http://dx.doi.org/10.1590/S0100-69162014000300003.

[52] C. Wang, L. Yin, L. Zhang, D. Xiang, R. Gao, Metal oxide gas sensors: sensitivity and influencing factors, Sensors 10 (2010) 2088–2106, http://dx.doi.org/10.3390/s100302088.

[53] G.F. Fine, L.M. Cavanagh, A. Afonja, R. Binions, Metal oxide semi-conductor gas sensors in environmental monitoring, Sensors 10 (2010) 5469–5502, http://dx.doi.org/10.3390/s100605469.

[54] G. Korotcenkov, S.H. Han, B.K. Cho, Material design for metal oxide chemiresistive gas sensors, J. Sens. Sci. Technol. 22 (2013) 1–17, http://dx.doi.org/10.5369/JSST.2013.22.1.1.

[55] T.-Y. Chen, H.-I. Chen, C.-S. Hsu, C.-C. Huang, J.-S. Wu, P.-C. Chou, et al., Characteristics of ZnO nanorods-based ammonia gas sensors with a cross-linked configuration, Sens. Actuators B Chem. 221 (2015) 491–498, http://dx.doi.org/10.1016/j.snb.2015.06.122.

[56] S. Yoo, X. Li, Y. Wu, W. Liu, X. Wang, W. Yi, Ammonia gas detection by tannic acid functionalized and reduced graphene oxide at room temperature, J. Nanomater. 2014 (2014) 1–6, http://dx.doi.org/10.1155/2014/497384.

[57] O.N. Oliveira Jr, T.A.T. Neves, F.V. Paulovich, M.C.F. de Oliveira, Where chemical sensors may assist in clinical diagnosis exploring big data, Chem. Lett. 43 (2014) 1672–1679, http://dx.doi.org/10.1246/cl.140762.

[58] F.V. Paulovich, M.L. Moraes, R.M. Maki, M. Ferreira, O.N. Oliveira, M.C.F. de Oliveira, Information visualization techniques for sensing and biosensing, Analyst 136 (2011) 1344–1350, http://dx.doi.org/10.1039/c0an00822b.

[59] M.L. Moraes, L. Petri, V. Oliveira, C.A. Olivati, M.C.F. De Oliveira, F.V. Paulovich, et al., Detection of glucose and triglycerides using information visualization methods to process impedance spectroscopy data, Sens. Actuators B Chem. 166–167 (2012) 231–238, http://dx.doi.org/10.1016/j.snb.2012.02.046.

[60] S. Ji, Y. Li, M. Yang, Gas sensing properties of a composite composed of electrospun poly(methyl methacrylate) nanofibers and in situ polymerized polyaniline, Sens. Actuators B Chem. 133 (2008) 644–649, http://dx.doi.org/10.1016/j.snb.2008.03.040.

[61] G.D. Khuspe, S.T. Navale, D.K. Bandgar, R.D. Sakhare, M.A. Chougule, V.B. Patil, SnO2 nanoparticles-modified polyaniline films as highly selective, sensitive, reproducible and stable ammonia sensors, Electron. Mater. Lett. 10 (2014) 191–197, http://dx.doi.org/10.1007/s13391-013-3096-0.

[62] Y. Yang, X. Yang, W. Yang, S. Li, J. Xu, Y. Jiang, Porous conducting polymer and reduced graphene oxide nanocomposites for room temperature gas detection, RSC Adv. 4 (2014) 42546–42553, http://dx.doi.org/10.1039/C4RA06560C.

[63] C. Xiang, D. Jiang, Y. Zou, H. Chu, S. Qiu, H. Zhang, et al., Ammonia sensor based on polypyrrole-graphene nanocomposite decorated with titania nanoparticles, Ceram. Int. 41 (2015) 6432–6438, http://dx.doi.org/10.1016/j.ceramint.2015.01.081.

[64] D.K. Bandgar, S.T. Navale, M. Naushad, R.S. Mane, F.J. Stadler, V.B. Patil, Ultra-sensitive polyaniline-iron oxide nanocomposite room temperature flexible ammonia sensor, RSC Adv. 5 (2015) 68964–68971, http://dx.doi.org/10.1039/C5RA11512D.

[65] Y. Li, H. Ban, M. Yang, Highly sensitive NH3 gas sensors based on novel polypyrrole-coated SnO2 nanosheet nanocomposites, Sens. Actuators B Chem. 224 (2015) 449–457, http://dx.doi.org/10.1016/j.snb.2015.10.078.

[66] S. Bai, Y. Tian, M. Cui, J. Sun, Y. Tian, R. Luo, Polyaniline@SnO2 heterojunction loading on flexible PET thin film for detection of NH3 at room temperature, Sens. Actuators B Chem. 226 (2016) 540–547, http://dx.doi.org/10.1016/j.snb.2015.12.007.